AD-A179 244 A NEW METHOD OF MAGNETIC BASEMENT-DEPTH DETERMINATION 1/1
(U) NAVAL OCEANOGRAPHIC OFFICE NSTL STATION MS
D R BRACEY ET AL. NOV 86 NOO-TR-296

UNCLASSIFIED F/G 8/14 NL

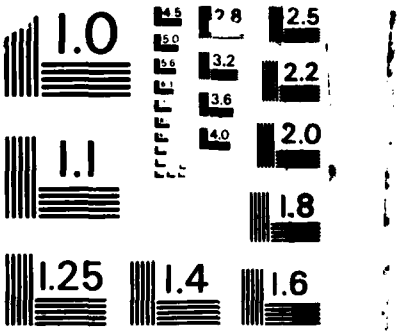

MICROCOPY RESOLUTION TEST CHART

NATIONAL BUREAU OF STANDARDS - 1963

Naval Oceanographic Office

Bay St. Louis,
NSTL,
Mississippi 39522-5001

Technical Report
TR-296
November 1986

TR-296

A NEW METHOD OF MAGNETIC BASEMENT-DEPTH DETERMINATION

DEWEY R. BRACEY
DONALD L. SHIEL
JOHN E. WEAVER

Approved for public release;
distribution unlimited.

Prepared under the authority of
Commander,
Naval Oceanography Command

UNCLASSIFIED
SECURITY CLASSIFICATION OF THIS PAGE

AD-A179 244

REPORT DOCUMENTATION PAGE

1a REPORT SECURITY CLASSIFICATION UNCLASSIFIED	1b RESTRICTIVE MARKINGS
2a SECURITY CLASSIFICATION AUTHORITY	3 DISTRIBUTION / AVAILABILITY OF REPORT Approved for public release; distribution unlimited
2b DECLASSIFICATION / DOWNGRADING SCHEDULE	
4 PERFORMING ORGANIZATION REPORT NUMBER(S) TR 296	5 MONITORING ORGANIZATION REPORT NUMBER(S)
6a NAME OF PERFORMING ORGANIZATION Code 8222 U.S. Naval Oceanographic Office 6b OFFICE SYMBOL (*If applicable*)	7a NAME OF MONITORING ORGANIZATION Commander, Naval Oceanography Command
6c ADDRESS (*City, State, and ZIP Code*) Bay St. Louis NSTL, MS 39522-5001	7b ADDRESS (*City, State, and ZIP Code*) Bay St. Louis NSTL, MS 39529-5000
8a NAME OF FUNDING / SPONSORING ORGANIZATION U.S. Naval Oceanographic Office 8b OFFICE SYMBOL (*If applicable*)	9 PROCUREMENT INSTRUMENT IDENTIFICATION NUMBER
8c ADDRESS (*City, State, and ZIP Code*) Bay St. Louis NSTL, MS 39522-5001	10 SOURCE OF FUNDING NUMBERS PROGRAM ELEMENT NO / PROJECT NO / TASK NO / WORK UNIT ACCESSION NO

11 TITLE (*Include Security Classification*)
A NEW METHOD OF MAGNETIC BASEMENT-DEPTH DETERMINATION

12 PERSONAL AUTHOR(S)
Bracey, Dewey, R.; Donald L. Shiel; and John E. Weaver

13a TYPE OF REPORT	13b TIME COVERED	14 DATE OF REPORT (*Year, Month, Day*)	15 PAGE COUNT
Technical Report	FROM _____ TO _____	November 1986	26

16 SUPPLEMENTARY NOTATION

17 COSATI CODES			18 SUBJECT TERMS (*Continue on reverse if necessary and identify by block number*)
FIELD	GROUP	SUB-GROUP	Magnetic basement, depth determination, geomagnetism, geophysics; Juan de Fuca area, Andaman Sea area, magnetic source depth

19 ABSTRACT (*Continue on reverse if necessary and identify by block number*)

Using band-pass-filtered, low-level aeromagnetic data, an algorithm has been empirically developed to relate magnetic anomaly half-wavelengths to magnetic basement depths. This simple, rapid source-depth determination method makes no assumptions as to magnetic source-body shape or magnetization. Instead, the method uses the principle that the closer an observer is to the source of a magnetic anomaly, the shorter the wavelength of that anomaly will be. Tests in two magnetically dissimilar geographic areas show that the method produces valid results, yielding magnetic basement contours that conform to the shape of bathymetry or seismically determined basement, and values that are within 200 - 300 meters of those determined by these latter methods.

20 DISTRIBUTION / AVAILABILITY OF ABSTRACT	21 ABSTRACT SECURITY CLASSIFICATION
☐ UNCLASSIFIED/UNLIMITED ☒ SAME AS RPT ☐ DTIC USERS	UNCLASSIFIED
22a NAME OF RESPONSIBLE INDIVIDUAL	22b TELEPHONE (*Include Area Code*) / 22c OFFICE SYMBOL

DD FORM 1473, 84 MAR — 83 APR edition may be used until exhausted. All other editions are obsolete.

SECURITY CLASSIFICATION OF THIS PAGE

☆ U.S. Government Printing Office: 1986—607-044

UNCLASSIFIED

TABLE OF CONTENTS

LIST OF FIGURES

Figure Page

INTRODUCTION

One of the fundamental properties of magnetic anomalies used for basement-depth determination is wavelength. A decision was made to test the possibility of using this property to develop an algorithm for rapid, automated, source-depth determinations that would be independent of source-body shape or any magnetization assumptions.

METHODOLOGY

For an empirical comparison of anomaly wavelength to basement depth, total magnetic intensity data filtered with the 63-Point HTA .08-.6 HZ bandpass filter (figure 1) were selected. Filter weights are given in the appendix. The reason for using the filtered rather than the actual total-intensity data was twofold. The filtered data have a clear-cut zero base line (figure 2) allowing unambiguous automated determination of positive and negative peak values for wavelength determination. In the computation process it was found that high-frequency noise of ±0.25-0.5 nT amplitude in the filtered data, as shown in figure 2, caused some erroneous peak-value selection. It was necessary to edit the filter profiles carefully to remove these erroneous values. The second reason for using the filtered data is that wavelengths at the high and low ends of the frequency spectrum which might bias depth determinations, and which are of no interest for this particular application, will be removed. An additional advantage of using this filter is that low-frequency, high-amplitude natural magnetic-field fluctuations are excluded from the data, leaving only those short-period fluctuations less than about 1.0 nT amplitude in the sampled data, as shown in figure 3.

The area selected for determining the empirical relationship of anomaly wavelength to magnetic source depth was the Juan de Fuca region off the coast of Washington (figure 4). Survey tracks flown by the Naval Oceanographic Office (NAVOCEANO) spaced at 3 nm in the eastern and western parts of the area and 6 nm in the central area were flown at an altitude of 150 meters above sea level (ASL) and at ground speeds of approximately 240 kns in an E-W direction nearly perpendicular to the strike of basement features. Data sample rate was 4 Hz. Note that the linear magnetic anomalies are sea-floor spreading anomalies originating at the Juan de Fuca spreading axis. Magnetic inclination in this region is approximatley 70°N.

Comparisons (figure 2) were made of half-wavelengths (which yield twice as many data points for subsequent computations as do full-wavelength measurements), to charted bathymetry, corrected for estimated sediment cover, and to seismic refraction and reflection depths to basement in areas of thick sedimentation. These seismic basement depths were obtained from numerous

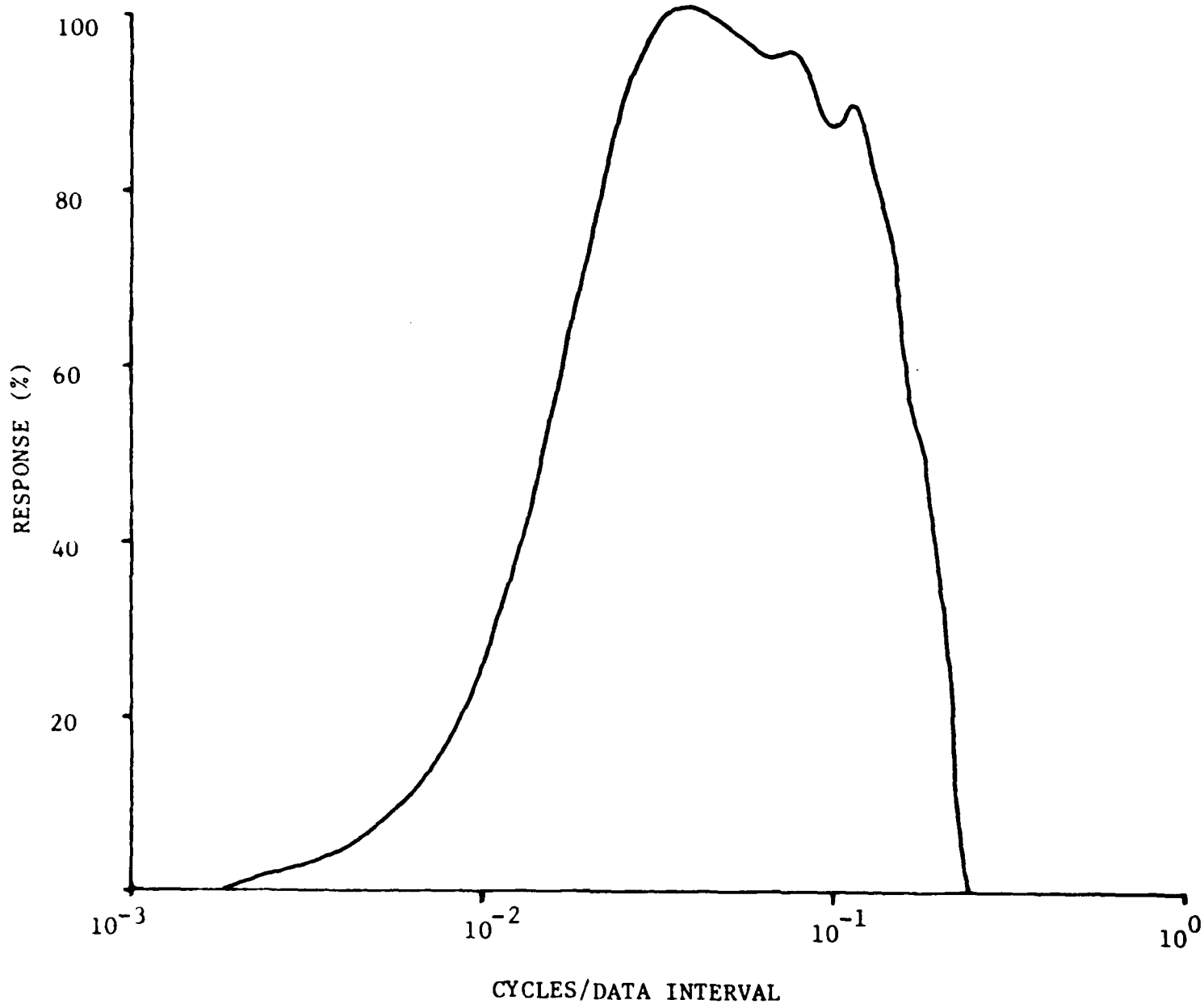

FIGURE 1. AMPLITUDE RESPONSE OF 63-POINT HTA .08 – .6 Hz BAND-PASS FILTER .

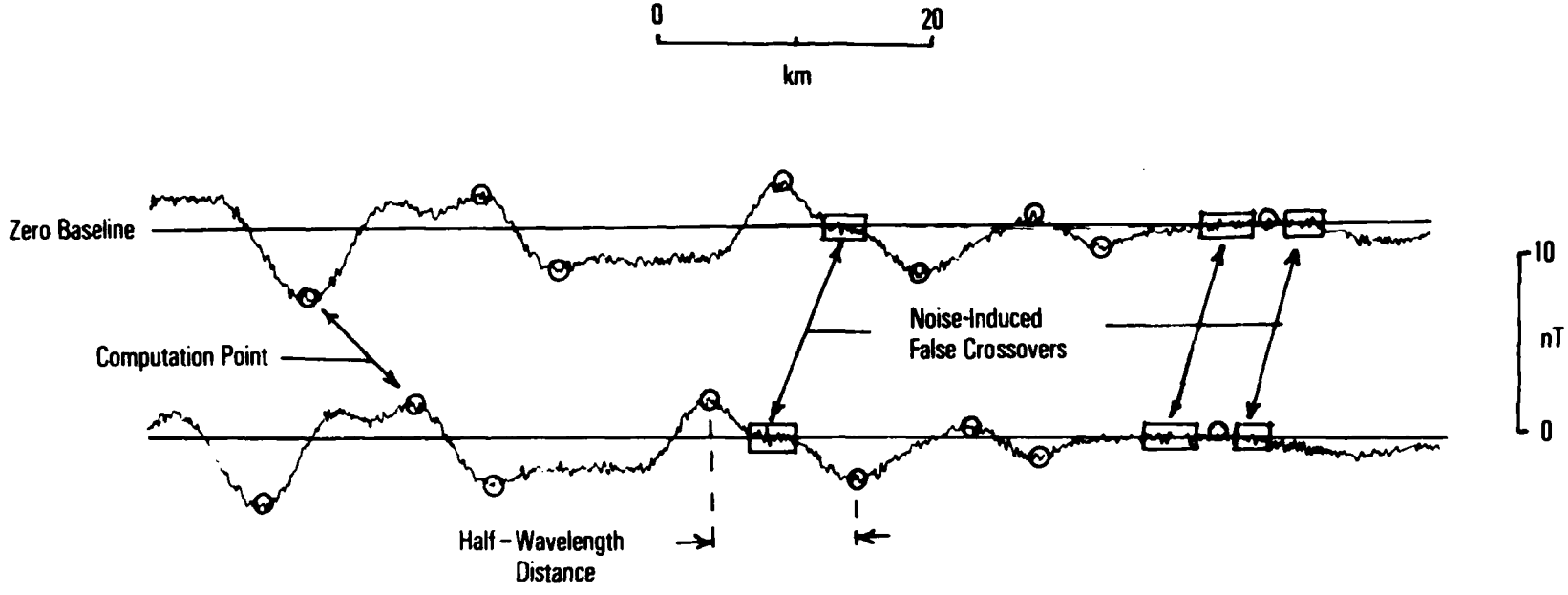

FIGURE 2. EXAMPLE OF 63-POINT HTA .08 – .6 Hz BAND-PASS FILTER OUTPUT PROFILE SHOWING COMPUTATION POINTS FOR HALF-WAVELENGTH DETERMINATION AND THE NOISE-INDUCED FALSE CROSSOVERS.

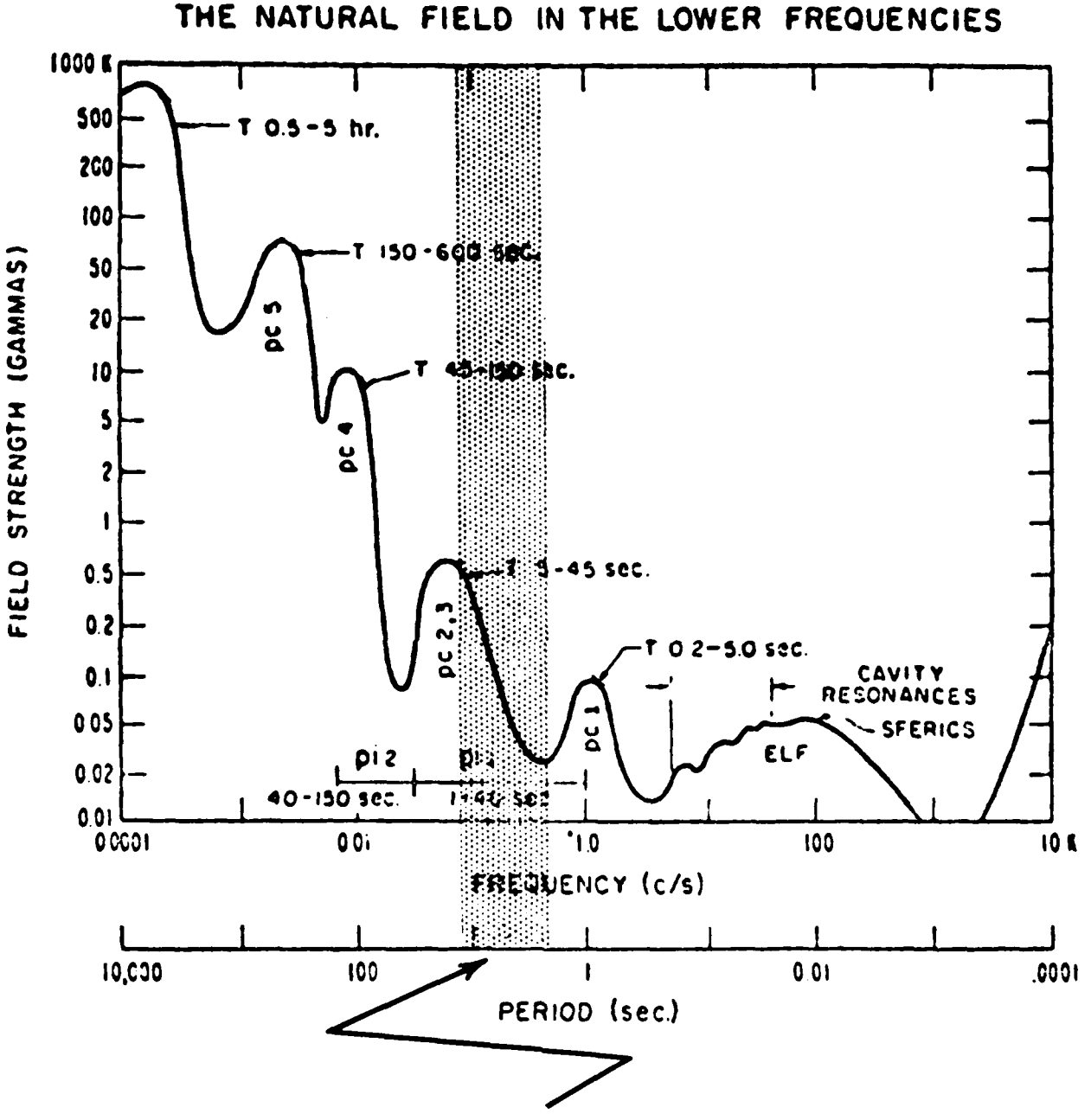

FIGURE 3. RELATIONSHIP OF THE .08 – .6 Hz BAND-PASS FILTER TO NATURALLY OCCURRING MAGNETIC DISTURBANCES (CAMPBELL, 1966).

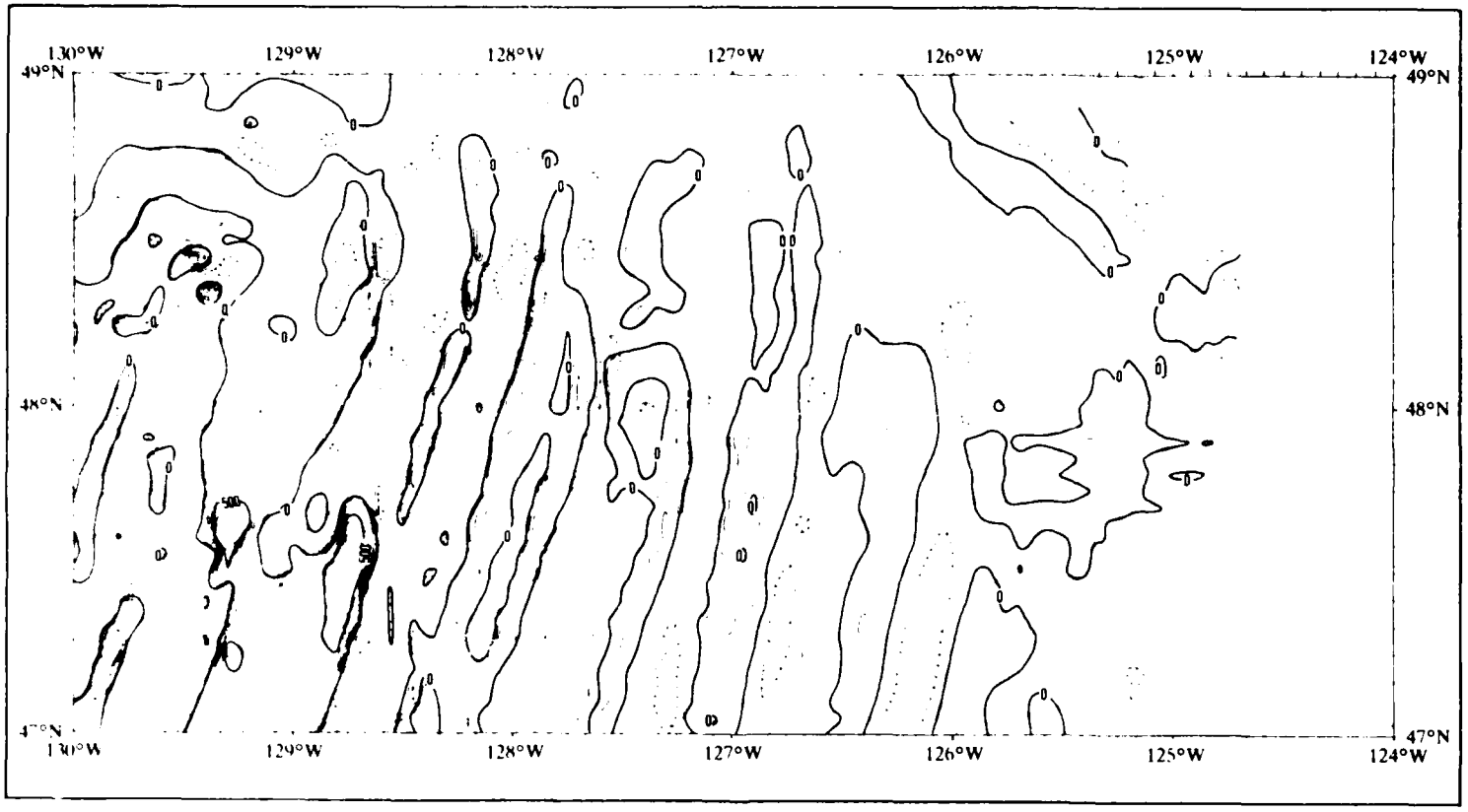

FIGURE 4. AEROMAGNETIC SURVEY OF THE JUAN DE FUCA AREA. (Residual Intensity Contours. Contour Interval 100nT.).

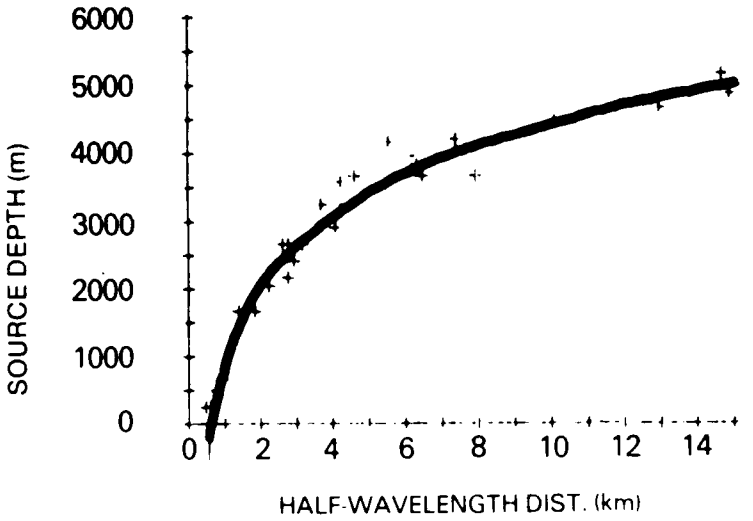

SOURCE/DF SS MS F
TOTAL 24.
REG 1. 536.3
RESID 231769624.9 76940.2
R SQUARE = 0.959

YHAT = 1032.561 + 1475.969LOG X

X(I)	Y(I)	YHAT	RESIDUALS
0.75	500.00	607.95	-107.95
14.63	5150.00	4992.70	157.30
4.63	3650.00	3294.57	355.43
4.26	3600.00	3171.64	428.36
3.15	2650.00	2726.09	-76.09
2.78	2150.00	2541.67	-391.67
1.85	1650.00	1940.56	-290.56
2.92	2400.00	2614.19	-214.19
5.56	4150.00	3564.73	585.27
12.96	4650.00	4813.80	-163.80
2.78	2650.00	2541.67	106.33
1.39	1650.00	1518.60	131.40
2.22	2050.00	2209.66	-159.66
7.96	3650.00	4094.35	-444.35
4.07	2900.00	3104.30	-204.30
6.48	3650.00	3790.74	-140.74
0.93	650.00	925.45	-275.45
0.46	250.00	-113.57	363.57
2.96	2400.00	2634.27	-234.27
14.82	4890.00	5011.74	-121.74
3.70	3250.00	2963.62	286.38
4.26	3150.00	3171.64	-21.64
10.10	4450.00	4445.79	4.21
2.59	2650.00	2437.18	212.82
7.40	4200.00	3986.68	213.32

FIGURE 5. LOGARITHMIC EXPRESSION DERIVED FROM EMPIRICAL OBSERVATIONS

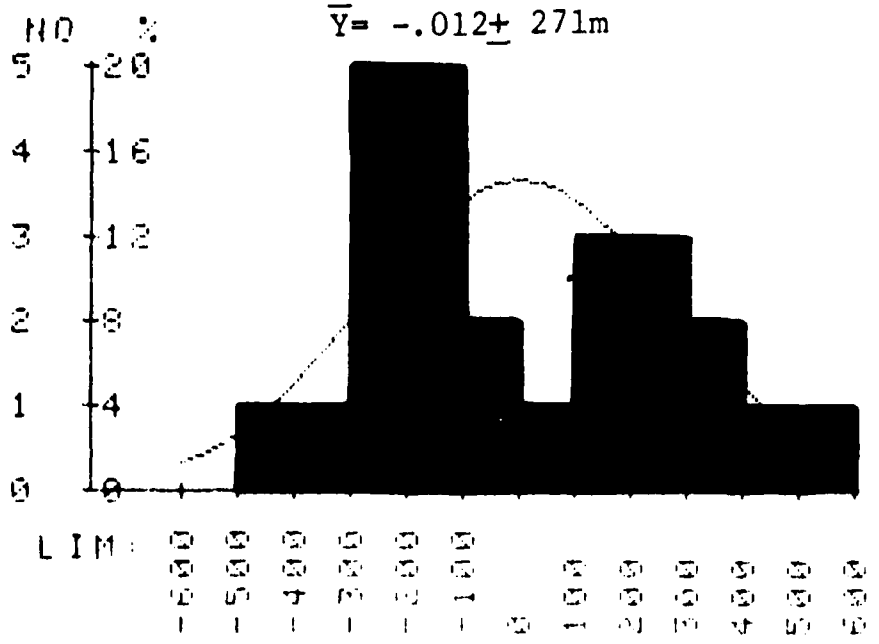

CELL STATISTICS

CELL#	LOWER LIMIT	NUMBER OF OBS	%RELATIVE FREQUENCY
2	-500.00	1	4.00
3	-400.00	1	4.00
4	-300.00	5	20.00
5	-200.00	5	20.00
6	-100.00	2	8.00
7	0.00	1	4.00
8	100.00	3	12.00
9	200.00	3	12.00
10	300.00	2	8.00
11	400.00	1	4.00
12	500.00	1	4.00

FIGURE 6. HISTOGRAM AND NORMAL DISTRIBUTION OF RESIDUAL MAGNETIC BASEMENT-DEPTH ERRORS.

published sources (Bernard, 1978; Barr, 1974; Carson and McManus, 1969; McManus et al., 1972; Shor et al., 1968).

The results of 25 such determinations are shown in figure 5. X is anomaly half-wavelength in kilometers and Y is basement depth in meters. As can be seen, the observed data are fitted by a logarithmic expression of the form Y = A + B * LN(X), where A = 1033 and B = 1476. A histogram of resididual error (figure 6), together with the normal distribution, showns a standard deviation of residual error of ±271 meters. This residual error is considered to be quite reasonable and some of it may be attributed to erroneous assumptions or judgements of sediment-thickness values.

A computer program was developed to locate the filtered-data peaks and troughs, correct for aircraft altitude, and compute the intervening distance. The logarithmic function was then applied to this distance to obtain a series of source-depth determinations along each E-W flight path. These data were then gridded at 3-minute intervals for machine contouring.

TEST RESULTS

1. Juan de Fuca Area

Figure 7 is the resulting basement-depth chart of the Juan de Fuca area contoured at a 500-meter interval. Note that the data can be gridded at any desired interval, but our limited experience has shown that gridding at less than the track-spacing interval introduces small-scale complexity that may or may not be desirable. Of course, grid and contour intervals are based on the magnitude of features one wishes to see, but unless survey track spacing is sufficiently dense, selecting too small an interval for either may introduce nonexistent small-scale complexity in machine-contoured data.

From comparison with charted bathymetry (figure 8) and the limited available seismic data, we found that this basement-depth chart is probably accurate to within 200-300 meters. Consider the complex and diverse basement depths and morphology in this area revealed by figure 7:

a. An active, though heavily sedimented, sea-floor spreading center,

b. High-relief basement beneath the bathymetrically smooth Cascadia Basin,

c. Basement plunging to more than 7-km depths as it enters the subduction zone off the Washington coast, and

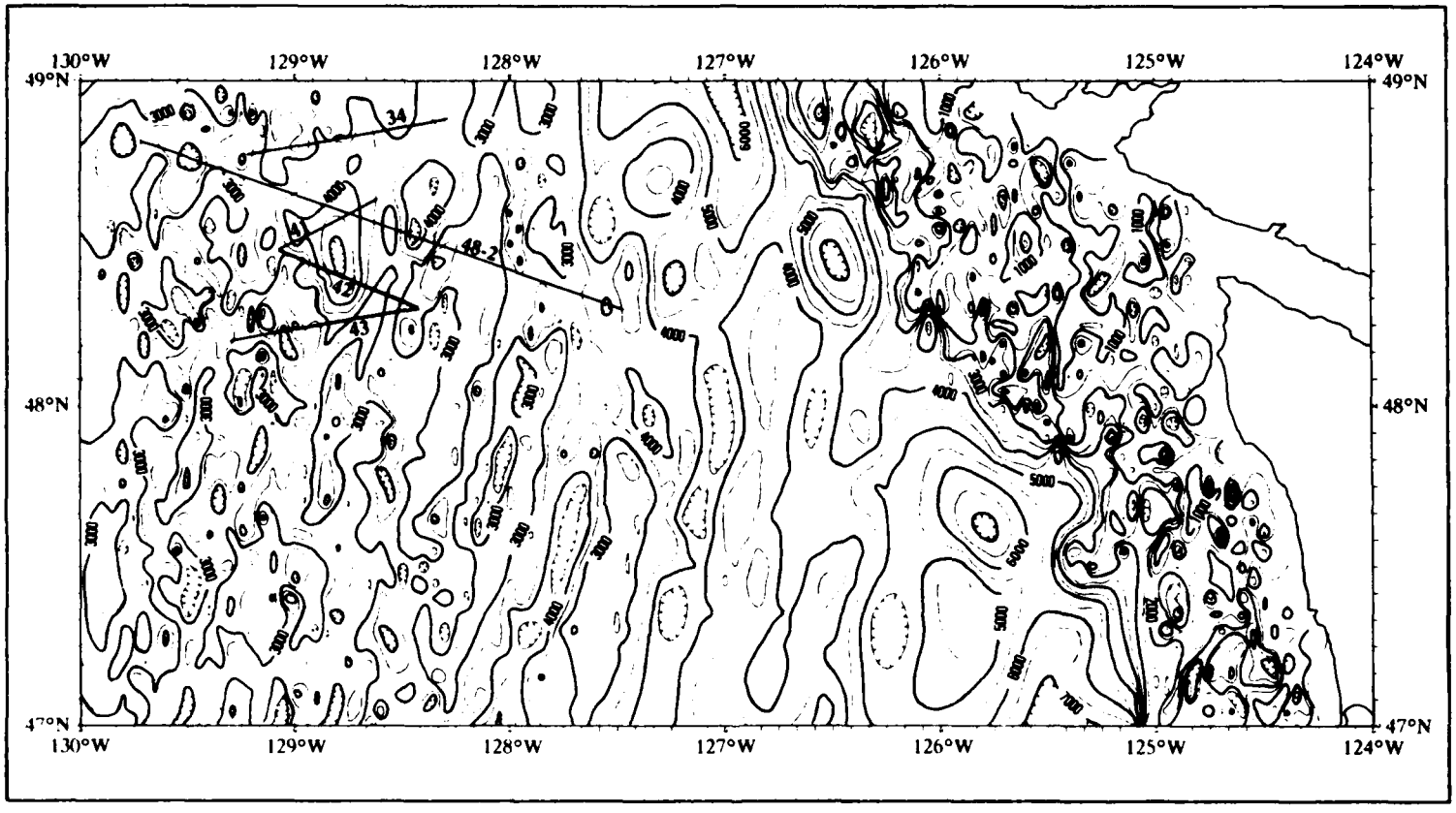

FIGURE 7. MAGNETIC BASEMENT CONTOURS OF THE JUAN DE FUCA AREA. NUMBERED LINES ARE LOCATIONS OF PROFILES SHOWN IN FIG. 9. (Contours in Meters B.S.L. Contour Interval 500m. Contour Grid Interval 3 min.).

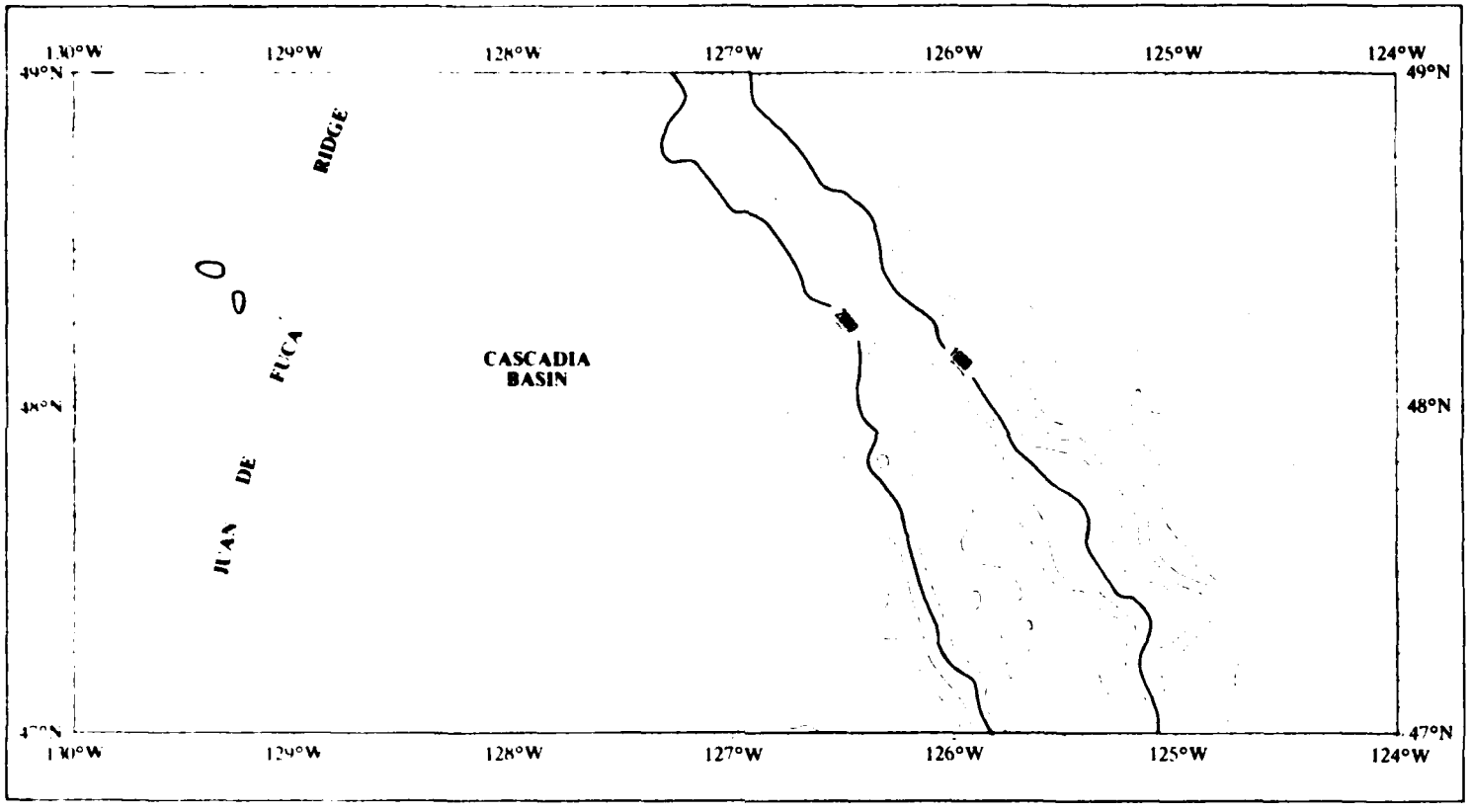

FIGURE 8. COMPUTER-GENERATED BATHYMETRIC CHART OF THE JUAN DE FUCA AREA. (Contour Interval 200m.).

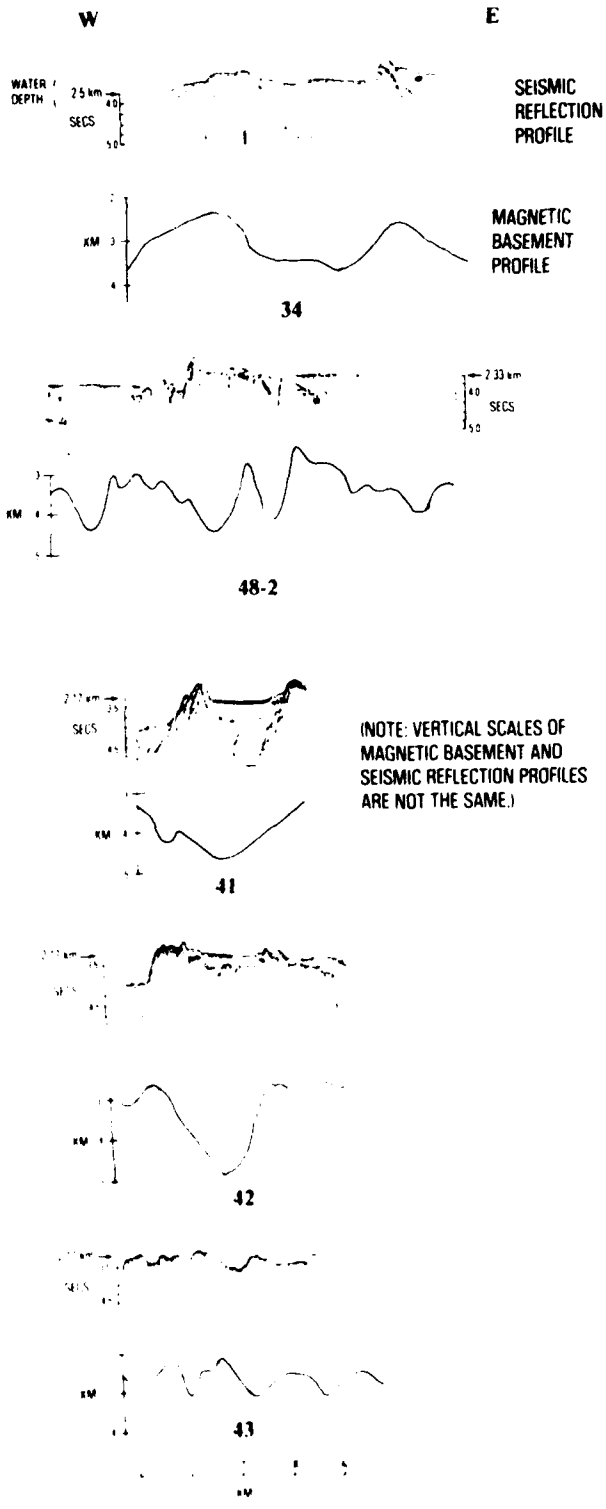

FIGURE 9. SEISMIC REFLECTION PROFILES (FROM McMANUS ET AL., 1972) LOCATED IN FIG. 7 COMPARED TO MAGNETIC BASEMENT-DEPTH PROFILES CONSTRUCTED FROM THE CONTOURS OF FIG. 7 AT THE SAME LOCATIONS.

d. Thick continental slope and shelf turbidite deposits probably intermixed with layers of volcanic detritus from eruptions of the nearby Olympic mountains which give rise to the relatively shallow and complex magnetic basement contours shown on the continental shelf.

Figure 9 compares seismic-reflection profiles, located in figure 7, to magnetic basement-depth profiles constructed from the contours of magnetic-basement depth at the seismic-profile location. Even though the actual magnetic tracks were not flown in the same direction or location as the seismic tracks, the correspondence in detail is quite remarkable. Only one magnetic-basement profile (line 42) shows substantial difference from the seismic profile. While only speculation, this difference may result from a thin layer of recent magma erupted from the active Juan de Fuca ridge onto a thick sediment accumulation in the magnetically defined trough. This layer would serve as a strong seismic reflector, but would not necessarily obscure the deeper magnetic basement.

2. Andaman Sea Area

A second test was conducted with aeromagnetic data collected by NAVOCEANO in an area of the Andaman Sea off the west coast of the Malay Peninsula (figure 10). This area is located on the magnetic equator, and magnetic inclination is negligible. It is also partly underlain by 100-m.y. crust of continental affinity, including acidic igneous rocks (which probably have little or no magnetization) encountered in wells drilled near the center of the area. Again, aircraft altitude was 150 meters ASL and ground speed was about 240 kns. Tracks were flown at 6-m spacing normal to the coast (E-W).

Basement depths were again determined using the logarithmic function, gridded at 9-minute intervals and contoured at 500-meter intervals (figure 11). When compared to charted bathymetry (figure 12), it is obvious that the salient features (ridges and troughs) are present in both, but that the magnetic basement is deeper (figure 11), reflecting a thick cover of sediment and/or nonmagnetic igneous rock. The magnetic basement also exhibits considerable morphological complexity in the form of buried basins and ridges not reflected in the bathymetry.

Total depths of wells drilled in the area are also known. Only two wells (3637 m and 2491 m) reached igneous rock, described as an "acid igneous complex" that is probably either nonmagnetic or very weakly magnetized compared to the underlying magnetic basement. Most of the other wells bottom in sedimentary rocks of varying lithology well above the charted magnetic basement depths. The exception is the 3810-m well, indicating magnetic basement at that location is at least 400 m too shallow.

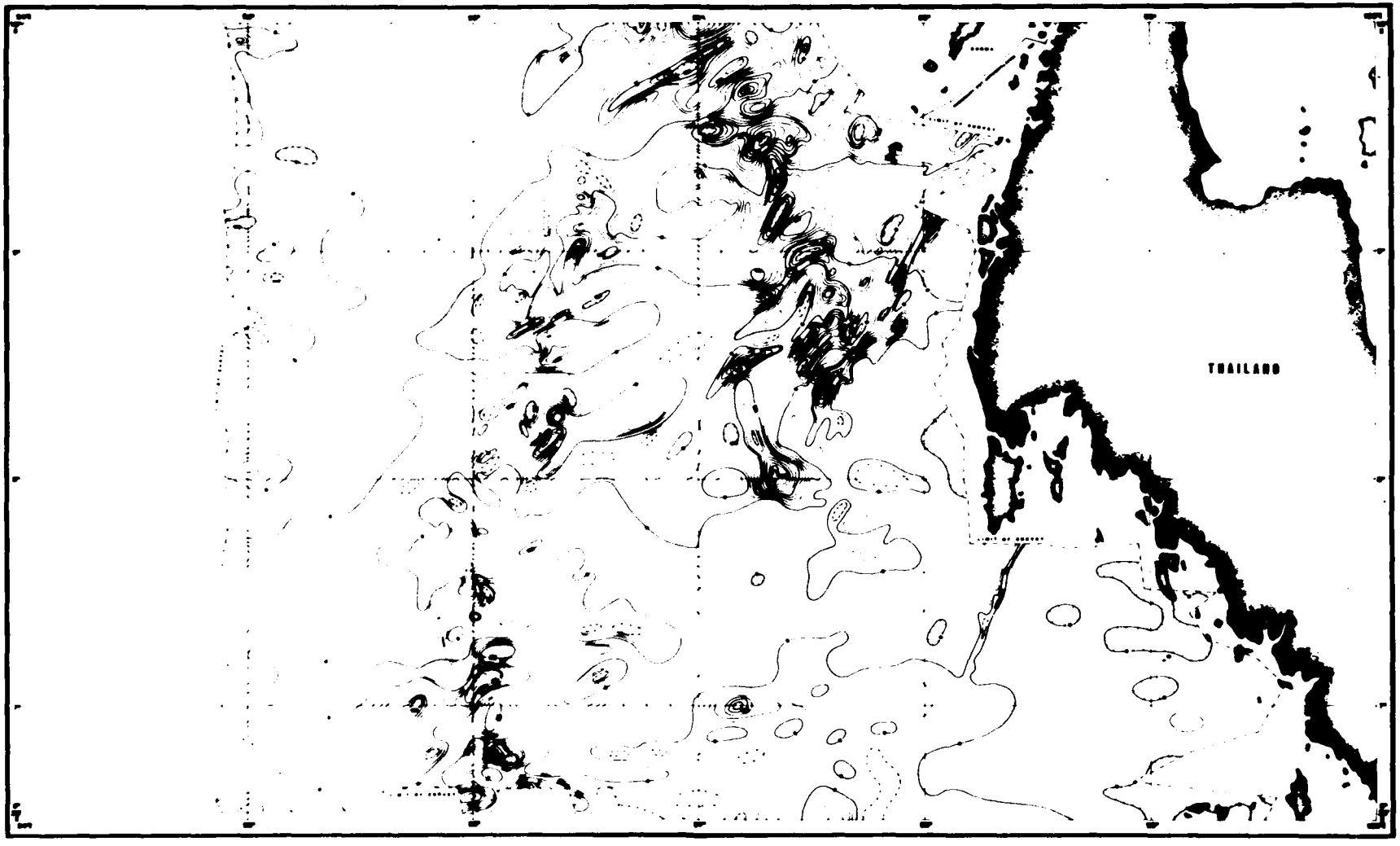

FIGURE 10. AEROMAGNETIC SURVEY OF AN AREA IN THE ANDAMAN SEA. (Residual Intensity Contours. Contour Interval 20nT.) .

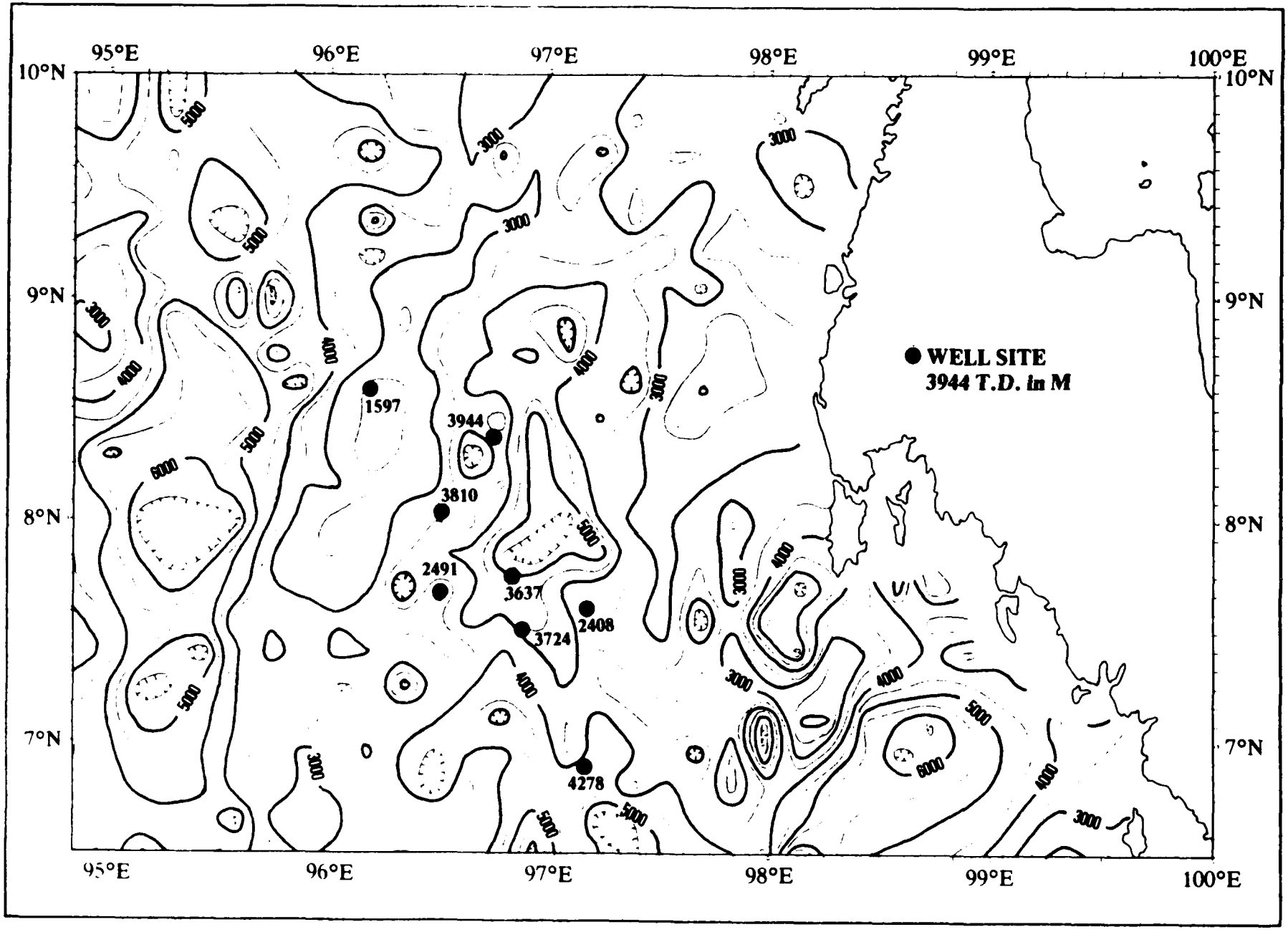

FIGURE 11. MAGNETIC BASEMENT CONTOURS OF THE ANDAMAN SEA AREA. (Contours in Meters B.S.L. Contour Interval 500m. Contour Grid Interval 9 min. Well Sites with Depths in Meters Shown by Solid Circles [From ASCOPE TECH. Committee, 1985]).

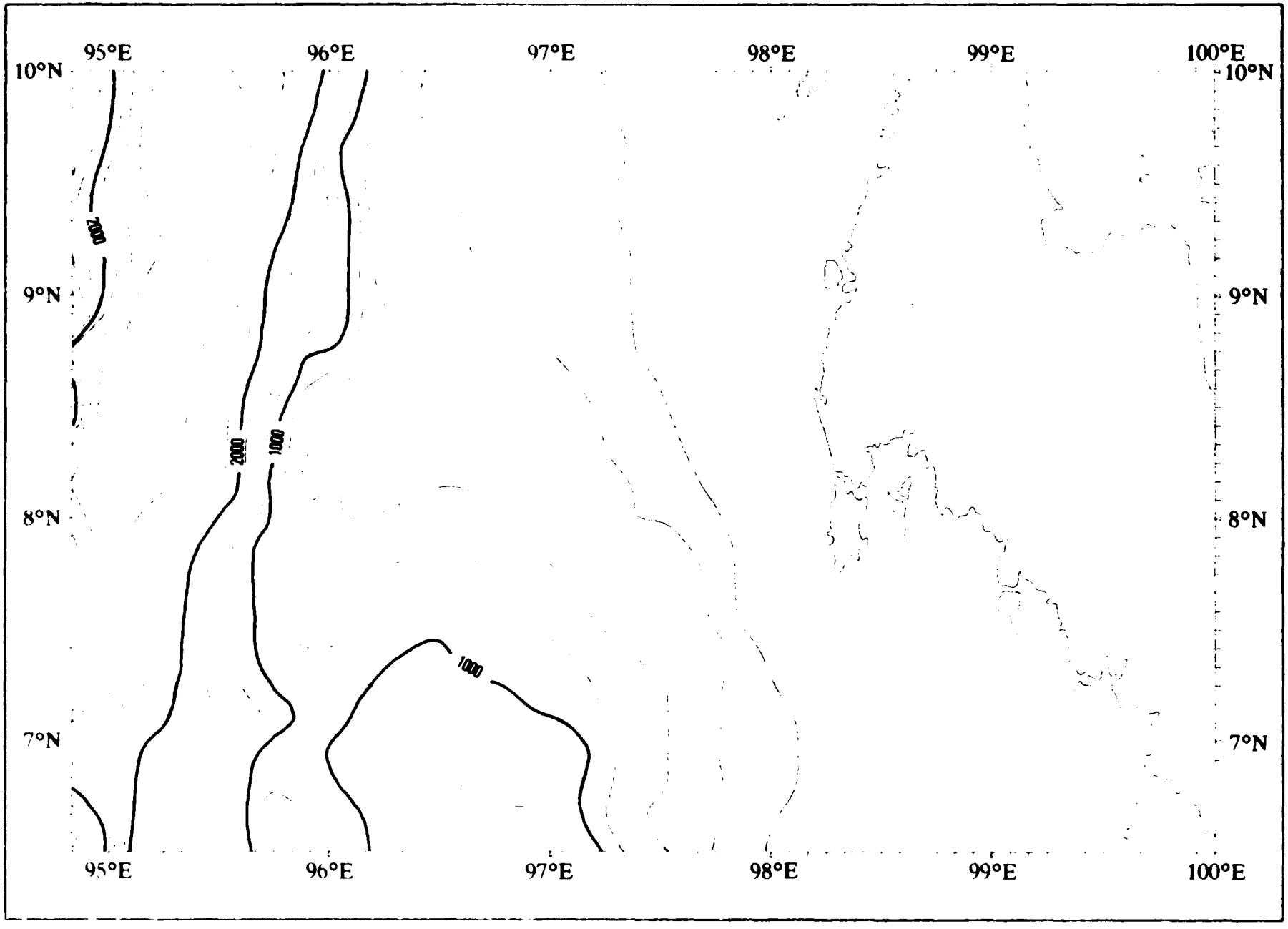

FIGURE 12. COMPUTER-GENERATED BATHYMETRIC CHART OF THE ANDAMAN SEA AREA. (Contour Interval 200m.).

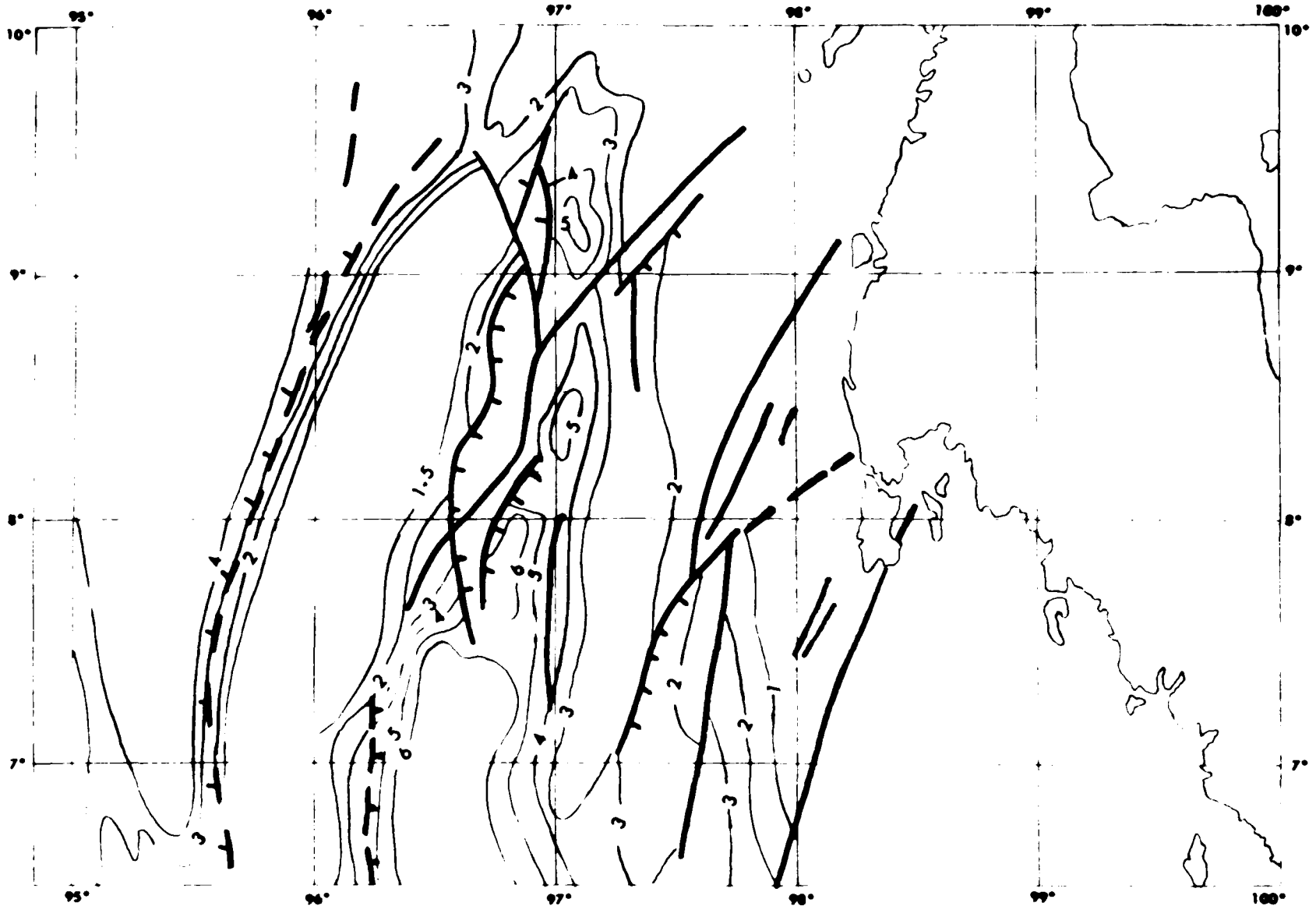

FIGURE 13. ANDAMAN SEA AREA ACOUSTIC BASEMENT CHART AND FRACTURES IN THE SEDIMENT COLUMN. (Depths in km B.S.L. [From ASCOPE Tech. Committee, 1985]).

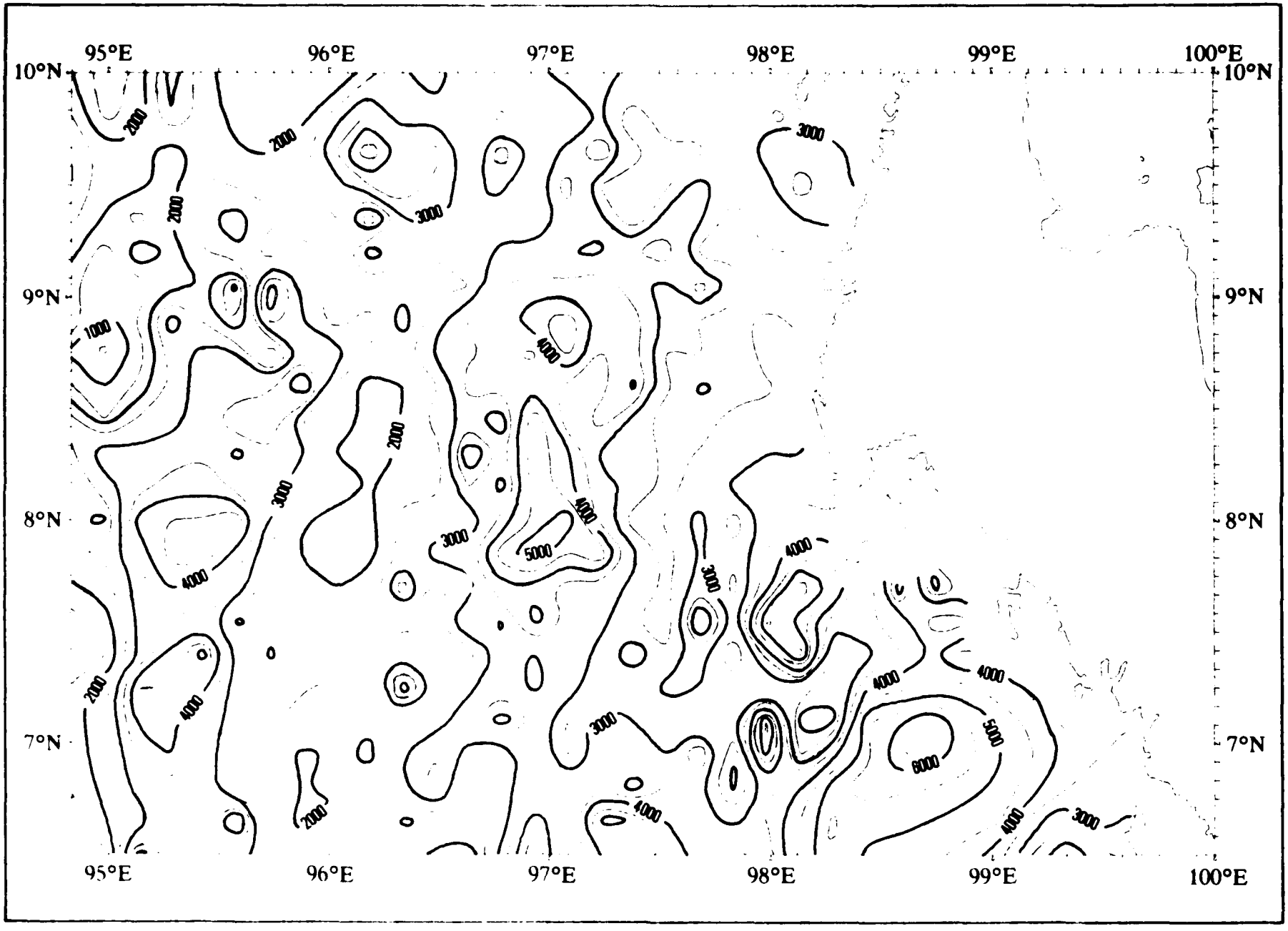

FIGURE 14. ANDAMAN SEA AREA SEDIMENT THICKNESS CHART (Bathymetry Minus Magnetic Basement. Contour Interval 500m.).

An acoustic basement chart of the area, which is based on an unknown distribution of seismic reflection data in addition to the well information, is shown in figure 13. Keep in mind that acoustic basement is the first hard refelctor which, except in deep-ocean areas, is generally not the same as magnetic basement. As can be seen, the general shape of the two basement surfaces is the same. The magnetic basement chart is much more detailed, reflecting the denser data sampling resulting from the detailed magnetic survey. The fractures shown in the acoustic basement chart are reflected to the magnetic basement chart (figure 11) in the form of discontinuities, steep gradients and lineations. There are probably many more fractures in the magnetic basement that would not be seen in the acoustic basement chart, since basement fractures propagating up through the sediments would be a function of fracture age and existing sedimentary cover at the time of fracture.

In figure 14, the simplicity of obtaining sediment-thickness values (bathymetry minus magnetic basement) is illustrated. The digital bathymetric data used in the construction of figure 12 are simply gridded at the same interval as the magnetic basement grid (9 minutes in this case) and the two are subtracted. The resultant sediment-thickness grid values can then be machine contoured at any desired interval.

CONCLUSIONS

These results show the validity and utility of this simple, rapid method of determining magnetic basement depths. It should be recognized that only in ocean basins, where sediment cover is relatively thin and the underlying basaltic layer is both acoustic and magnetic basement, can magnetic basement be roughly equated to bathymetry. On continental shelves and slopes, only in exceptional cases, such as on the Washington continental shelf where there appear to be shallow layers of magnetized volcanic detritus mixed with the thick sedimentary deposits, will there be any correlation between magnetic basement depths and shelf/slope bathymetric depths. This method offers great potential as a reconnaissance tool for the determination and location of seamounts, ridges, and other bathymetric features for subsequent bathymetric development, as well as for the delineation of subbottom relief in the ocean basins for acoustic applications.

REFERENCES

ASCOPE Technical Committee, The Stratigraphic Correlation Study of the Andaman Sea-Strait of Malacca, ASEAN Council on Petroleum, Technical Report No. 4, 1985.

Barnard, W.D., The Washington Continental Slope: Quaternary Tectonics and Sedimentation, Mar. Geol., Vol 27, pp. 79 - 114, 1978.

Barr, S.M., Structure and Tectonics of the Continental Slope West of Southern Vancouver Island, Can. Jour. of Earth Sciences, Vol 11, pp. 1187 - 1199, 1974.

Campbell, W.H., A Review of the Equatorial Studies of Rapid Fluctuations in the Earth's Magnetic Field, Ann. Geophys., Vol. 22, p. 492, 1966.

Carson, Bob, and D.A. McManus, Seismic Reflection Profiles Across Juan de Fuca Canyon, Jour. Geophys. Res., Vol. 74, pp. 1052 - 1060, 1969.

Davis, E.E., C.R.B. Lister, and B.T.R. Lewis, Seismic Structure of the Juan de Fuca Ridge: Ocean Bottom Seismometer Results from the Median Valley, Jour. Geophys. Res., Vol. 81, pp. 3541 - 3555, 1976.

McManus, D.A., M.L. Holmes, Bob Carson, and S.M. Barr, Late Quaternary Tectonics, Northern End of Juan de Fuca Ridge (Northeast Pacific), Mar. Geol., Vol. 12, pp. 141 - 164, 1972.

Shor, G.G., Jr., P. Dehlinger, H.K. Kirk, and W.S. French, Seismic Refraction Studies Off Oregon and Northern California, Jour. Geophys. Res., Vol. 73, pp. 2175 - 2194, 1968.

APPENDIX

63-POINT HTA .08 - .6 Hz BAND-PASS FILTER WEIGHTS

1. -.26895-02	17. -.11061-01	33. .23893+00	49. -.16155-01
2. -.41671-02	18. -.15586-01	34. .75501-01	50. -.14209-01
3. -.35590-02	19. -.24699-01	35. -.47133-01	51. -.10920-01
4. -.14962-02	20. -.27490-01	36. -.69101-01	52. -.97764-02
5. -.75096-03	21. -.21630-01	37. -.34456-01	53. -.94730-02
6. -.20933-02	22. -.19090-01	38. -.12824-01	54. -.77340-02
7. -.36163-02	23. -.26696-01	39. -.21091-01	55. -.54282-02
8. -.42823-02	24. -.31431-01	40. -.31431-01	56. -.42823-02
9. -.54282-02	25. -.21091-01	41. -.26696-01	57. -.36163-02
10. -.77340-02	26. -.12824-01	42. -.19090-01	58. -.20933-02
11. -.94730-02	27. -.34456-01	43. -.21630-01	59. -.75096-03
12. -.97764-02	28. -.69101-01	44. -.27490-01	60. -.14962-02
13. -.10920-01	29. -.47113-01	45. .24699-01	61. -.35590-02
14. -.14209-01	30. .75501-01	46. -.15586-01	62. -.41671-02
15. -.16155-01	31. .23893+00	47. -.11061-01	63. -.26895-02
16. -.13628-01	32. .31562+00	48. -.13628-01	

CNO (OP-006, OP-212, OP-952D, OP-953, PME-124)	5
COMNAVOCEANCOM	3
DARPA	2
DMA	1
DMAAC	2
DMAHTC	2
DNL	2
DTIC	12
NAVAIRDEVCEN	2
NAVELEX	2
NAVMINEWARCEN	2
NAVPGSCOL	2
NGSDC/NOAA	2
NOAA	2
NORDA	7
NRL	3
NUSC	2
OCEANAV	2
OCNR	2
ONR	3
USGS	2
USGS Menlo Park	2
USGS Denver	2

END

5-87

DTIC